Solvation Effects on the A-Band Photodissociation of Dibromomethane: Turning a Photodissociation into a Photoisomerization†

Xuming Zheng, Wai Ming Kwok,‡ and David Lee Phillips*

Department of Chemistry, The University of Hong Kong, Pokfulam Road, Hong Kong

Received: March 28, 2000; In Final Form: July 18, 2000

We have obtained A-band resonance Raman spectra of dibromomethane in the gas and solution phase and nanosecond time-resolved resonance Raman spectra of dibromomethane photoproducts. The A-band resonance Raman spectra suggest the short-time dynamics are similar to other dihalomethanes that are known to have direct photodissociation reactions in the gas phase. Several power dependent A-band resonance Raman bands were tentatively assigned to the C−Br stretch overtone progression of the CH_2Br radical which has a strong absorption band that is coincident with the A-band resonance Raman excitation wavelength. Two-color nanosecond time-resolved resonance Raman spectra (266.0 nm pump/341.5 nm probe) were obtained and comparison of the vibrational frequencies to the results for density functional theory calculations indicate that the iso-CH_2Br−Br species is mainly responsible for the transient photoproduct absorption band ∼360 nm. Our preliminary results for A-band photoexcitation of dibromomethane in conjunction with previously reported diiodomethane results suggest that solvation effects (probably via recombination of the CH_2Br and Br fragments within a solvent cage) lead to noticeable production of the isodibromomethane photoisomerization photoproduct observed in the nanosecond time-resolved resonance Raman spectra.

Introduction

Dihalomethanes such as diiodomethane and dibromomethane have been used as reagents for cyclopropanation reactions with alkenes.[1−8] Diiodomethane has long been employed for cyclopropanation reactions via activation of the diiodomethane reagent by a Zn−Cu couple in the Simmons−Smith reaction[1] or ultraviolet photoexcitation.[2−5] More recently dibromomethane has been shown to be an effective reagent for cyclopropanation reactions employing variations of the Simmons−Smith reaction with ultrasound irradiation,[6] $TiCCl_4$ catalysis,[7] or electrochemical synthesis with a Zn anode.[8] Dihalomethanes have also been of increasing interest in atmospheric chemistry since they may be an important source of natural organoiodine and organobromine compounds emitted into the atmosphere.[9−13] A recent study assessed the importance of dibromomethane, diiodomethane and bromoiodomethane as possible sources for reactive halogens in the troposphere and in the marine boundary layer.[14]

The absorption cross sections of dibromomethane in the ultraviolet has been experimentally measured by several groups.[14−16] Dibromomethane has only one broad absorption band above 210 nm that most likely arises from n → σ^* transitions (from a nonbonding electron on the Br atom to an antibonding σ^* orbital on the C−Br bond).[17,18] Presumably, photoexcitation of dibromomethane within this absorption band in the gas phase results in direct C−Br bond cleavage similar to the A-band photodissociation reactions previously found for diiodomethane[19−21] and other haloalkanes.[22−38] While the ultraviolet photodissociation of diiodomethane has been investigated by a variety of experimental techniques in the gas phase,[19−21,39−48] solution phase,[48−52] and in low-temperature solids,[53−60] there has been relatively few corresponding studies reported for dibromomethane.[14,53,55,56] In this paper we report A-band Resonance Raman spectra of dibromomethane in the gas and solution phase in order to elucidate the qualitative features of the Franck−Condon region dynamics of the photodissociation reaction. We also report transient resonance Raman experiments in the solution phase. These solution phase experiments indicate formation of an isodibromomethane photoproduct within nanoseconds after photoexcitation. We compare our present results for dibromomethane with those of diiodomethane and discuss their differences and similarities. Our results for dibromomethane suggest that solvation effects (likely via recombination of the CH_2Br + Br fragments within the solvent cage) leads to appreciable photoisomerization to give an isodibromomethane (iso-CH_2Br−Br) photoproduct.

Experiment

CH_2Br_2 (99%) and spectroscopic grade cyclohexane (99.9+%) were used to prepare samples for the resonance Raman experiments and time-resolved resonance Raman experiments. Sample concentrations were in the 0.15 to 0.20 M range for all of the different resonance Raman experiments. The resonance Raman apparatus and methods have been described in detail elsewhere[48,49,61−66] so only a short account will be given here. The harmonics of a Nd:YAG laser and their hydrogen Raman shifted laser lines provided the excitation wavelengths for the resonance Raman experiments. A backscattering geometry was used to excite a flowing liquid stream of sample. Reflective optics were used to collect the resonance Raman scattered light and image it through a depolarizer and entrance slit to a 0.5 m spectrograph. The grating of the spectrograph dispersed the light onto a liquid nitrogen cooled CCD detector that accumulated the signal for about 1 to 2 min before being read out to an

† Part of the special issue "C. Bradley Moore Festschrift".

‡ Present address: Department of Chemistry, Imperial College of Science, Technology and Medicine, Exhibition Road, London SW7 2AY, U.K. and Central Laser Facility, Rutherford Appleton Laboratory, Chilton, Didcot, Oxfordshire OX11 0QX, U.K.

10.1021/jp001168+ CCC: $19.00
Published on Web 11/09/2000

interfaced PC computer. About 20 to 30 of these readouts were added together to get the resonance Raman spectrum.

The gas phase experiments used the same excitation and detection apparatus as the solution phase experiments. A heated reservoir of liquid and vapor dibromomethane connected to a heated pipet was used in the gas phase experiments. Dry nitrogen was flowed through the sample reservoir to take away some dibromomethane vapor with it through the pipet nozzle. The excitation laser beam was loosely focused (~2 mm diameter) near the exit of the pipet nozzle. The laser power was kept low to avoid interference from photoproduct bands. The excitation laser light was not noticeably reduced by the vapor sample and sample reabsorption of the resonance Raman scattering was minimal for the vapor phase experiments.

The time-resolved resonance Raman apparatus and methods have been detailed previously[67−71] so only a brief description is given here. The time-resolved experiments made use of the same equipment as the resonance Raman experiments. The fourth harmonic (266 nm) of a nanosecond pulsed Nd:YAG laser was used for the pump excitation wavelength and the second Stokes hydrogen Raman shifted laser line (341.5 nm) of the fourth harmonic was used for the probe excitation wavelength in the transient resonance Raman experiments. A near collinear geometry was used focus the pump and probe laser beams onto a flowing liquid jet of sample. The Raman signal was collected and detected in a manner similar to that used for the resonance Raman experiments. Pump only, probe only, background scan and pump−probe transient Raman spectra were obtained. The solvent and parent dibromomethane Raman bands were excised from the pump−probe transient spectrum by subtracting a probe only spectrum (the pump only and background scan displayed no noticeable bands in the probe spectral region).

The known vibrational frequencies of the cyclohexane solvent Raman bands (for solution phase spectra) and mercury emission lines as well as the oxygen and nitrogen Raman bands (for the vapor phase spectra) were used to calibrate the Raman shifts of the resonance Raman spectra. The solution phase spectra were corrected for any remaining sample reabsorption[72] and the solvent Raman bands were removed via subtraction of an appropriately scaled solvent spectrum. The wavelength dependence of the detection system response was corrected in all of the Raman spectra using spectra of an intensity calibrated deuterium or tungsten lamp. Portions of the corrected spectra were fit to a baseline plus a sum of Lorentzians to obtain the integrated areas of the resonance Raman bands.

Calculations

All of the density functional theory computations were done using the Gaussian program suite.[73] The complete geometry optimization and vibrational frequency calculations were determined analytically and employed a C_s symmetry constraint where the plane of symmetry contained the carbon atom and the bromine atom(s). The 6-311++G(3df,3pd) and Aug-cc-PVTZ basis sets[74,75] were used for the B3LYP density functional theory (DFT) computations for the optimized structures and vibrational frequencies. These basis sets were also used for the time-dependent density functional theory at random phase approximation[76] computations (TD(RPA)) to calculate the electronic transition energies.

Results and Discussion

Figure 1 shows absorption spectra of dibromomethane in the gas and solution phases (cyclohexane solvent) with the wavelength for the resonance Raman experiments displayed above the absorption spectra. The dashed lines in Figure 1 present a simple Gaussian deconvolution of the absorption spectra of dibromomethane. Figure 2 presents an overview of the 228.9 nm resonance Raman spectra of gas and solution phase (cyclohexane solvent) dibromomethane as well as an expanded view of the 1000 cm^{-1} to 3500 cm^{-1} region to more easily see the smaller Raman bands. Most of the intensity in the resonance Raman spectra of Figure 2 appear in progressions associated with three or four Franck−Condon active vibrational modes (the nominal Br−C−Br bend ν_4, the nominal Br−C−Br symmetric stretch ν_3, the nominal Br−C−Br antisymmetric stretch ν_8, and the nominal H−C−H bend ν_2). Table 1 lists the Raman shifts and intensities for the resonance Raman spectra displayed in Figure 2 for gas and solution phase dibromomethane. There are three moderate intensity Raman bands that display noticeable power dependence[77] in the gas and solution phase resonance Raman spectra (694, 1383, and 2062 cm^{-1}) which are attributed to a nominal C−Br stretch overtone progression of the CH_2Br radical. The CH_2Br radical has a moderately intense A-band absorption ~230 nm (8.8×10^{-18} cm^2/molecule)[78,79] that is overlapped with the parent CH_2Br_2 absorption band that we are investigating in this study. The infrared absorption spectra of the CH_2Br and CD_2Br radicals were observed in low-temperature Ar matrix studies[80,81] and the nominal C−Br stretch mode observed at 693 cm^{-1} displays good agreement with the power dependent Raman band progression we have tentatively assigned to the C−Br stretch overtone progression of the CH_2Br radical. We estimated an upper limit for the fraction of sample photoconverted using the following equation from refs 82 and 83:

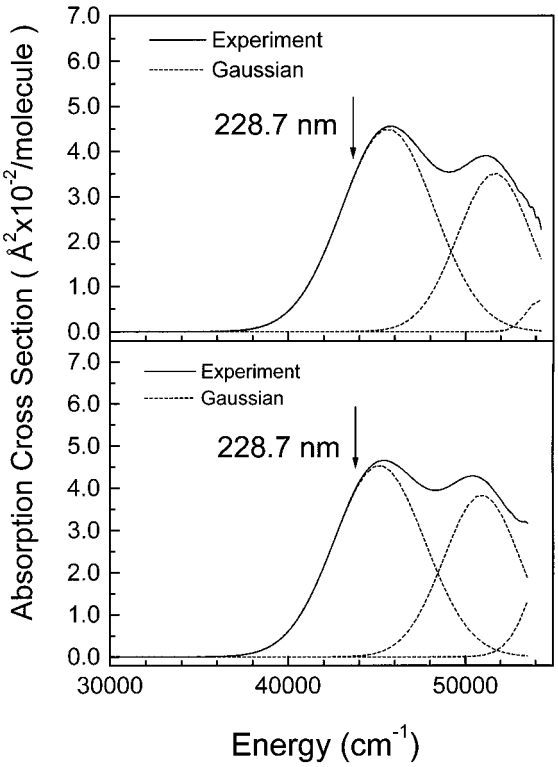

Figure 1. Absorption spectra of gas (top) and solution phase (bottom) dibromomethane. The dashed lines represent a simple Gaussian deconvolution of the absorption spectra. The wavelength (nm) for the resonance Raman experiments is shown above the spectra.

$$F_{\text{pulse}} = (2303E\epsilon\phi)/(\pi r^2 N_A)$$

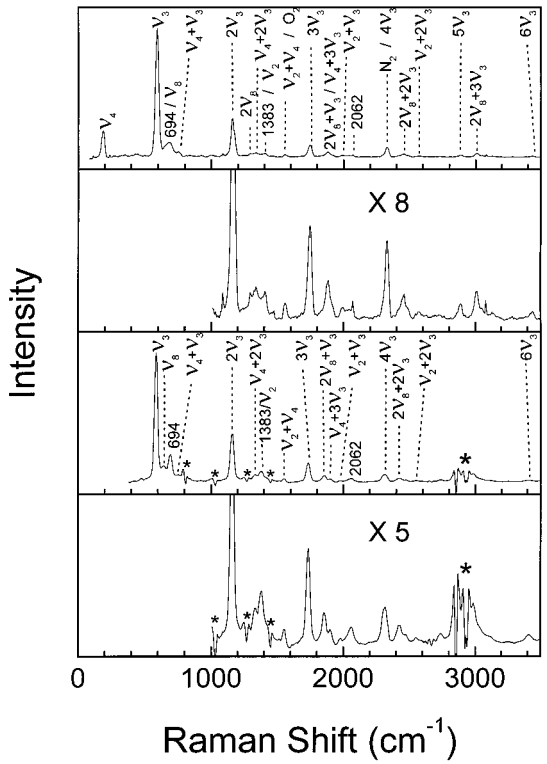

Figure 2. A-band resonance Raman spectra of dibromomethane in the gas (top) and solution (cyclohexane solvent; bottom) phases. An expanded view (×8 and ×5, respectively) of the gas and solution phase spectra is shown immediately below each of these spectra. The spectra have been intensity corrected and solvent subtracted. The tentative assignments for the larger Raman bands are shown above the spectra. Asterisks (*) label regions of the spectra where solvent subtraction artifacts are present and the pound sign (#) marks regions where laser line or stray light artifacts are found.

For the experimental conditions used to acquire the resonance Raman spectra in Figure 2 (228.7 nm excitation with 0.5 mW at 10 Hz $= 5 \times 10^{-5}$ J or $E = 5.76 \times 10^{13}$ 228.7 nm photons, $r = 0.05$ cm, $\epsilon = 1026$ M^{-1} cm^{-1}, $\phi = 1.0$, and $N_A = 6.02 \times 10^{23}$) we found an upper limit of 3% photoconversion of the sample. The CH_2Br radical has an absorption cross section ~230 nm of 8.8×10^{-18} cm^2/molecule[78,79] that is about 2.24 times larger than that of the parent dibromomethane molecule at 228.7 nm (~3.9×10^{-18} cm^2/molecule). Since the Raman cross section scales as the square of the absorption cross section the bromomethyl radical resonance Raman cross section is probably about 5 times larger than that of dibromomethane at ~228.7 nm. We observe <12% of the Raman intensity in the photoproduct bands and this is consistent with the <3% sample photoconversion upper limit. Apart from the modest intensity found for a few transient bromomethyl radical Raman bands, the resonance Raman intensities of the spectra in Figure 2 and measured absolute Raman cross section in the solution phase (Table 1) should be mainly indicative of the parent dibromomethane molecule. The details of the resonance Raman spectra of the CH_2Br radical photoproduct and its Franck−Condon region dynamics will be reported separately.[77]

We note that the dibromomethane A-band resonance Raman spectra have most of their intensity in the nominal Br−C−Br symmetric stretch overtone progression ($n\nu_3$). This progression accounts for most of the resonance Raman cross section and would be expected to determine most of the short-time photodissociation dynamics associated with the main transition of the A-band absorption of dibromomethane. The resonance Raman spectra in Figure 2 appear similar to the resonance Raman spectra (and presumably their Franck−Condon region dynamics as well) previously found from resonance Raman studies for other dihalomethanes that are known to have direct photodissociation of a C−X bond following A-band photoexcitation (where X = Br or I).[48,62,63,66] This and the intense overtone progression in the symmetric C−Br vibrational mode suggests that A-band excitation of dibromomethane leads to direct bond cleavage of the C−Br bond. The gas and solution phase A-band resonance Raman spectra are very similar to one another with the exception of some moderate intensity in bands associated with the Br−C−Br antisymmetric stretch mode in the solution phase which either do not appear or are much less intense in the gas phase. This may be due to some solvent induced symmetry breaking as has been previously observed in the diiodomethane system.[48,49] The fundamental of the X−C−X antisymmetric stretch and combination bands of this fundamental with other modes is substantially smaller in the A-band dibromomethane spectra compared to the diiodomethane spectra.[48] This suggests that degree of solvent induced symmetry breaking is less in dibromomethane than in diiodomethane. This could be due to the faster separation of the $CH_2X + X$ fragments in dibromomethane compared to diiodomethane which would lead to a shorter time spent in the Franck−Condon region and less solvent perturbation of the resonance Raman spectra. However, little is known about the energy partitioning associated with the A-band dibromomethane reaction so at this time we can only speculate about this.

We have done two-color nanosecond time-resolved resonance Raman spectroscopy experiments to help examine some of the photoproducts produced following A-band photoexcitation of dibromomethane in room temperature solutions. Figure 3 presents a typical 341.5 nm probe only Raman spectrum (A), a

TABLE 1: Experimental A-Band Resonance Raman Intensities for Gas and Solution (cyclohexane solvent) Phase Dibromomethane (for 228.7 nm excitation)

Raman bands	Raman shift[a] (cm^{-1})	intensities as absolute Raman cross sections ($\times 10^{-9}$ Å^2/molecule)	
		gas phase[c] exp[b]	soln phase exp[b]
ν_3	587 (576)	1.21	1.21
$2\nu_3$	1158	0.36	0.50
$3\nu_3$	c1734	0.12	0.20
$4\nu_3$	2312	0.10	0.11
$5\nu_3$	2880	0.02	c
$6\nu_3$	3438	0.01	0.04
ν_8	640 (637)		
$2\nu_8$	1290	0.01	*c*
$2\nu_8 + \nu_3$	1855	0.06	0.08
$2\nu_8 + 2\nu_3$	2423	0.04	0.05
$2\nu_8 + 3\nu_3$	3012	0.04	*c*
ν_4	179 (174)	0.24	*c*
$\nu_4 + \nu_3$	756	0.03	*c*
$\nu_4 + 2\nu_3$	1330	0.04	0.03
$\nu_4 + 3\nu_3$	1903	0.02	0.03
ν_2	1388 (1388)	0.03	
$\nu_2 + \nu_4$	1552	0.016	0.022
$\nu_2 + \nu_3$	1964	0.012	0.014

[a] Estimated uncertainties are about ±4 cm^{-1} for the Raman shifts. The Raman shifts for the gas phase Raman bands are shown first and the solution phase values are given in parentheses. [b] Intensities are based on integrated areas of peaks and solution phase absolute Raman cross section measurements (the listed values are in units of 10^{-9} Å^2/molecule). Estimated uncertainties are about 10% for intensities for 1.0 or higher, 15% for intensities 0.3−1.0 and 30% for intensities lower than 0.3. The gas phase values are only relative intensities (these have been scaled so that the ν_3 cross section is the same as the solution phase value). [c] These peaks are obscured by solvent subtraction artifacts and/or apparent transient Raman peaks.

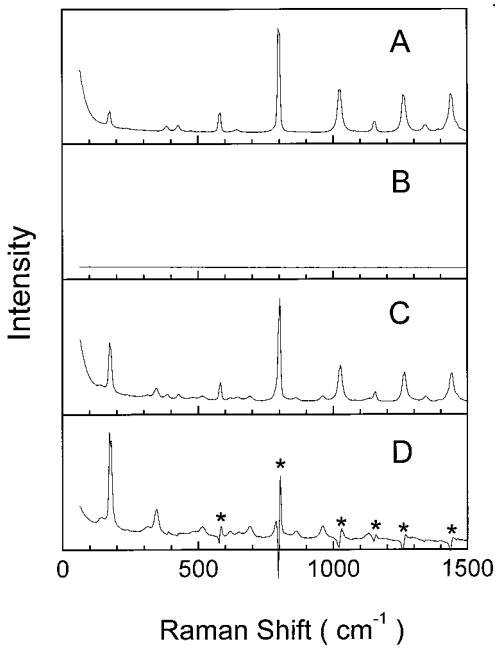

Figure 3. Examples of a typical 341.5 nm probe only Raman spectrum (A), 266.0 nm pump only spectrum in the probe wavelength region (B), a pump−probe Raman spectrum (C), and the resulting transient resonance Raman spectrum (D) of the dibromomethane photoproduct.

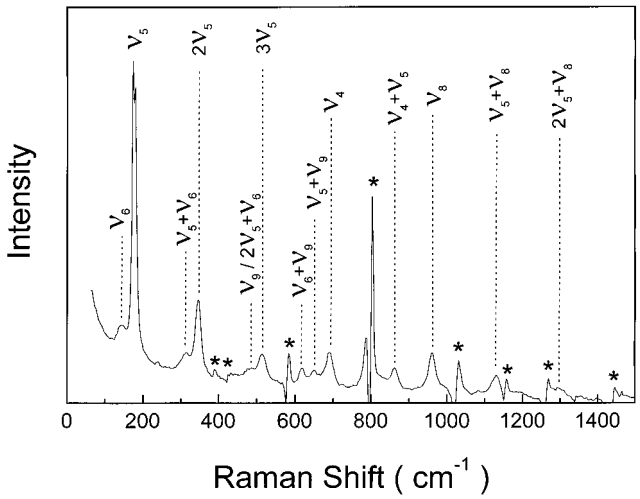

Figure 4. Transient resonance Raman spectra of the dibromomethane (CH_2Br_2) photoproduct obtained using a 266.0 nm pump and 341.5 nm probe excitation wavelengths. The time delay between the pump and probe beams was ∼0 ns.

266.0 nm pump only spectrum in the probe wavelength region (B), a pump−probe resonance Raman spectrum (C) and a transient resonance Raman spectrum of the photoproduct (D) obtained by subtracting the probe only and pump only spectra from the pump−probe spectrum. Figure 4 shows an expanded view of the transient resonance Raman spectrum of the dibromomethane photoproduct with the tentative assignments of the larger Raman bands indicated above the spectrum. The 266.0 nm pump wavelength is resonant with the red edge of the A-band absorption spectrum of dibromomethane and the probe wavelength is resonant with transient photoproduct absorption bands observed in low-temperature matrices.[53−59] Since we have a limited number of available hydrogen Raman shifted probe excitation wavelengths in the 320 nm to 380 nm wavelengths region using our current experimental apparatus we did not attempt to obtain an excitation profile across the

TABLE 2: Parameters for the Optimized Geometries Computed from the B3LYP Density Functional Theory Calculations for iso-CH_2Br_2, CH_2Br, and $CH_2Br_2^+$ Species (Bond Lengths in Å and Bond Angles in Degrees)

parameter	B3LYP/ 6-311++G(3df,3pd)	B3LYP/ Aug-cc-PVTZ
	iso-CH_2Br_2	
$C-Br_1$	1.767	1.768
Br_1-Br_2	2.672	2.674
$C-H_3$ and $C-H_4$	1.078	1.078
$C-Br_1-Br_2$	122.0	122.0
Br_1-C-H_3 and Br_1-C-H_4	118.0	118.1
$H_3-C-Br_1-Br_2$	−80.66	−80.68
$H_4-C-Br_1-Br_2$	80.66	80.68
	$CH_2Br_2^+$	
$C-Br_1$ and $C-Br_2$	1.946	1.946
$C-H_3$ and $C-H_4$	1.081	1.082
Br_1-C-Br_2	93.98	93.85
Br_1-C-H_3, Br_1-C-H_4, Br_2-C-H_3, and Br_2-C-H_4	110.9	110.9
H_3-C-H_4	117.0	116.9
$Br_1-C-Br_2-H_3$	−114.1	−114.1
$H_3-C-H_4-Br_1$	−128.5	−128.6
	CH_2Br	
$C-Br$	1.857	1.858
$C-H_1$ and $C-H_2$	1.075	1.075
$Br-C-H_1$ and $Br-C-H_2$	117.7	117.7
H_1-C-H_2	124.7	124.6
H_1-C-H_2-Br	180.0	180.0

∼360 nm transient absorption band. This would be interesting to do at some point and would likely reveal more about the nature of the transient electronic absorption transition. Ultraviolet, photoionization and radiolysis excitation of dibromomethane, diiodomethane and other dihalomethanes in low-temperature matrices leads to photoproducts that have a characteristic intense absorption band in the 320 nm to 450 nm region (∼360 nm for the photoproduct of dibromomethane and ∼370−385 nm for the photoproduct of diiodomethane for example) and a weaker absorption further to the red.[53−59] The characteristic photoproduct absorption band around 360 nm observed for dibromomethane following ultraviolet or photoionization excitation has been attributed to trapped electrons,[53] the $CH_2Br_2^+$ radical cation[57] or the isomer of dibromomethane (CH_2Br-Br).[55,56] The transient resonance Raman spectra displayed in Figure 3 (D) and Figure 4 have most of their Raman intensity in the fundamentals, overtones and combination bands of four or five Franck−Condon active modes whose fundamental Raman bands are at 960 cm^{-1}, 690 cm^{-1}, 480 cm^{-1}?, 176 and 146 cm^{-1}.

We have performed density functional theory calculations to find the optimized geometries, vibrational frequencies and electronic absorption transitions for the CH_2Br, $CH_2Br_2^+$ and iso-CH_2Br-Br species. Table 2 presents the parameters for the optimized geometries of CH_2Br, $CH_2Br_2^+$ and iso-CH_2Br-Br obtained from the B3LYP density functional theory computations. Table 3 compares the experimental frequencies found from the transient resonance Raman spectra (this study) with the calculated density functional theory results for iso-CH_2Br_2, $CH_2Br_2^+$, and CH_2Br. Examination of Table 3 shows the experimental vibrational frequencies of the Raman band fundamentals show reasonable agreement with those predicted for the iso-CH_2Br-Br species but not for the $CH_2Br_2^+$ radical cation or the CH_2Br radical which have been proposed as species for the photoproduct ∼360 nm absorption band. The CH_2Br species

TABLE 3: Comparison of the Experimental Vibrational Frequencies (cm^{-1}) Found from the Transient Resonance Raman Spectra (This Work) and Infrared Absorption Spectra (Refs 55 and 56) to the Calculated B3LYP Density Functional Theory Vibrational Frequencies[a]

vibrational mode		B3LYP/6-311++G(3df,3pd)	B3LYP/Aug-cc PVTZ	resonance Raman (this work)	infrared abs[55,56]
		CH_2Br-Br (CD_2Br-Br)			
A′	ν_1, CH_2 sym str	3154 (2277)	3152 (2275)		3030 (2213)
	ν_2, CH_2 scissor	1429 (1079)	1428 (1078)		1334 (1030)
	ν_3, C−Br str	861 (773)	858 (771)		(732)
	ν_4, CH_2 wag	740 (595)	738 (594)	690	684, 695
	ν_5, Br−Br str	180 (180)	180 (180)	176	
	ν_6, C−Br−Br bend	132 (123)	133 (124)	146	
A″	ν_7, CH_2 asym str	3294 (2452)	3286 (2456)		3156 (2384)
	ν_8, CH_2 rock	967 (725)	966 (724)	960	
	ν_9, CH_2 twist	469 (338)	468 (337)	480*	
		$CH_2Br_2^+$			
A_1	ν_1, CH sym str	3140 (2271)	3132 (2265)		
	ν_2, CH_2 def	1426 (1046)	1424 (1045)		
	ν_3, CBr sym str	627 (597)	626 (596)		
	ν_4, BrCBr bend	167 (167)	169 (168)		
B_1	ν_5, CH asym str	3259 (2433)	3247 (2424)		
	ν_6, CH_2 rock	871 (666)	873 (668)		
A_2	ν_7, CH_2 twist	1033 (733)	1032 (732)		
B_2	ν_8, CH_2 wag	1176 (880)	1172 (877)		
	ν_9, CBr asym str	531 (510)	528 (507)		
		CH_2Br			
A_1	ν_1, CH sym str	3175 (2286)	3172 (2284)		
	ν_2, CH_2 def	1382 (1030)	1382 (1029)		
	ν_3, C−Br str	703 (663)	703 (662)		
B_1	ν_4, CH_2 wag	157 (122)	152 (118)		
B_2	ν_5, CH asym str	3334 (2494)	3325 (2488)		
	ν_6, CH_2 rock	928 (693)	926 (691)		

[a] The corresponding vibrational frequencies for deutrated isodibromomethane are given in parentheses. Key: str = stretch; sym = symmetric; asym = asymmetric; def = deformation.

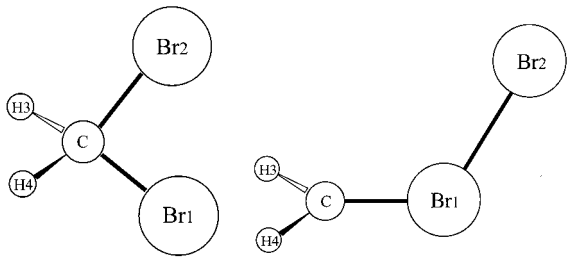

Figure 5. Schematic diagram of the geometry of dibromomethane and isodibromomethane.

and the $CH_2Br_2^+$ species have only one vibrational mode in the 100 cm^{-1} to 200 cm^{-1} region (at 152 and 169 cm^{-1} respectively). This does not agree with the experimental nanosecond time-resolved resonance Raman spectra in Figures 3 (D) and 4 that show two low-frequency modes at 176 and 146 cm^{-1} (these two modes have overtones and/or combination bands with each other and the other Franck−Condon active vibrational modes). However, the iso-CH_2Br-Br species (a simple schematic diagram of the geometry is given at the bottom of Figure 5) has two A_1 low-frequency vibrational modes (∼180 and 133 cm^{-1}) that correspond well to the experimental Raman fundamentals at 176 and 146 cm^{-1}. In addition, the other Franck−Condon active modes in the experimental resonance Raman spectra display reasonable agreement with the computed iso-CH_2Br-Br vibrational frequencies. Using the comparison of vibrational frequencies in Table 3, we make the following tentative assignments for the five Franck−Condon active modes observed in the time-resolved resonance Raman spectra: the nominal C−Br−Br bend ν_6, the nominal Br−Br stretch ν_5, the nominal CH_2 wag ν_4, the nominal CH_2 rock ν_8 and the nominal CH_2 twist ν_9 modes correspond to the experimental fundamentals at 146, 176, 690, ∼960, and ∼480 cm^{-1}, respectively. We note that the 690 cm^{-1} Raman fundamental band assigned to the nominal CH_2 wag ν_4 mode agrees well with the experimental band vibrational frequency and assignment found from infrared spectra obtained in low-temperature matrixes.[55,56] The differences in the resonance Raman band intensities and bandwidths in the experimental spectrum shown in Figure 4 were used to help make preliminary assignments of the ν_9 and ν_8 fundamentals and their combination bands. Our present results strongly indicate that the iso-CH_2Br-Br species is mainly responsible for the ∼360 nm absorption band observed following ultraviolet photoexcitation of dibromomethane in room-temperature liquid solutions.

We have previously used B3LYP time-dependent random phase (TD/RPA) computations to estimate electronic transition energies and oscillator strengths for CH_2I_2 and found reasonable agreement with the experimental spectra.[84] We have also done similar calculations for the electronic transitions of iso-CH_2Br-Br, $CH_2Br_2^+$ radical cation and CH_2Br radical and results for the singlet transitions are shown in Table 4. The $CH_2Br_2^+$ radical cation and CH_2Br radical species have no strong computed transitions in the 330 nm to 400 nm region where the ∼360 nm experimental absorption band occurs. However, the iso-CH_2Br-Br species has two intense transitions at 374 and 356 nm that correspond very well to the experimental absorption spectrum ∼360 nm associated with the photoproduct formed following ultraviolet photoexcitation of dibromomethane in condensed environments.[53,55−57] The nanosecond time-resolved resonance Raman spectra of the photoproduct reported here show that the iso-CH_2Br-Br species is responsible for the ∼360 nm transient absorption band seen after ultraviolet excitation of dibromomethane in liquid solutions (at least on the ns time scale) and this is consistent with the DFT computed electronic transition energies and oscillator strengths for iso-CH_2Br-Br.

TABLE 4: Electronic Absorption Transition Energies Obtained from Density Functional Theory Calculations for iso-CH_2Br_2, $CH_2Br_2^+$, and CH_2Br[a]

molecule	electronic absorption transition energies	
	URPA//UB3LYP/6-311++G(3df,3pd)	URPA//UB3LYP/Aug-cc-PVTZ
iso-CH_2Br_2	singlet transitions	
	399 nm (0.0002)	390 nm (0.0002)
	388 nm (0.3698)	374 nm (0.3380)
	369 nm (0.1066)	356 nm (0.1919)
	250 nm (0.0003)	249 nm (0.0001)
	222 nm (0.0047)	219 nm (0.0033)
	201 nm (0.1094)	201 nm (0.1005)
$CH_2Br_2^+$	1948 nm (0.1151)	1941 nm (0.1150)
	817 nm (0.0003)	814 nm (0.0003)
	648 nm (0.0000)	644 nm (0.0000)
	298 nm (0.0002)	298 nm (0.0001)
	216 nm (0.0478)	216 nm (0.0462)
CH_2Br	255 nm (0.0012)	255 nm (0.0011)
	197 nm (0.0000)	198 nm (0.0001)
	191 nm (0.0001)	194 nm (0.0000)

[a] Calculated transition oscillator strengths are in parentheses.

How does solvation lead to formation of the iso-CH_2Br-Br photoproduct species? To help address this question, it is useful to examine the more extensively studied diiodomethane photodissociation/photoisomerization reactions. Ultraviolet excitation of diiodomethane in the gas phase leads to cleavage of one C−I bond to give CH_2I and iodine atom photofragments.[19−21,43−45] Solution phase femtosecond transient absorption experiments[50−52] generally concur that the initial process is also C−I bond cleavage to produce CH_2I and iodine atom fragments (the very fast rise time observed in all of the femtosecond experiments). This is consistent with frequency domain resonance Raman investigations of the Franck−Condon region short-time dynamics.[46−49] While all three femtosecond transient absorption experiments observe very similar behavior of a fast rise component (a few hundred femtoseconds) followed by a fast decay component (several hundreds of femtoseconds) and then a slower (3−10 ps) rise component, the interpretations of these results have varied due to the species assigned to the transient absorptions.[50−52] We recently performed nanosecond time-resolved resonance Raman experiments to observe the photoproduct (that has a characteristic ∼385 nm transient absorption) produced following ultraviolet photoexcitation of diiodomethane in solution.[85] Our time-resolved resonance Raman spectra in conjunction with density functional theory calculations clearly demonstrated that isodiiodomethane (iso-CH_2I-I) photoproduct is produced from ultraviolet photoexcitation of diiodomethane in room-temperature liquids on the nanosecond time scale and is associated with the characteristic ∼385 nm transient absorption band.[85] These results suggest that insofar as the transient absorption band ∼385 nm observed on the ultrafast time scale is the same as that seen on the nanosecond time scale, the interpretation of the femtosecond transient absorption spectra proposed by Akesson[52] is probably correct (ultraviolet photoexcitation of diiodomethane in solution leads to fast C−I bond cleavage to form CH_2I and I fragments, the fragments then interact with the solvent cage leading to some recombination to produce a hot isodiodomethane photoproduct that then vibrationally cools to give the isodiiodomethane photoproduct observed at longer times). We note that the other two femtosecond transient absorption studies[50,51] also interpreted the first two steps of the mechanism following ultraviolet photoexcitation of diiodomethane in liquids as fast C−I bond cleavage to give CH_2I and I fragments and these fragments then interact with the solvent cage to give some geminate recombination and some escape of the fragments. It appears that the geminate recombination of the CH_2I and I photofragments within the solvent cage leads to appreciable amounts of the isodiiodomethane photoproduct.

Our present results resonance Raman experiments show that CH_2Br photoproduct and isodibromomethane (iso-CH_2Br-Br) photoproduct are both observed within nanoseconds following photoexcitation of the A-band absorption of dibromomethane in cyclohexane solution. The A-band resonance Raman intensity spectra for dibromomethane indicates that the Franck−Condon region dynamics lead mostly to lengthening of the C−Br bonds and likely dynamics similar to that observed for A-band diiodomethane and other dihalomethanes[48,62,63] that are known to have direct photodissociation reactions in the gas phase.[19−21,43−45,86−89] Using this information and results for the closely related diiodomethane system,[50−52] we propose the following preliminary hypothesis for the primary photochemistry steps for A-band photoexcitation of dibromomethane in liquid solutions: the C−Br bond breaks in a direct manner to give CH_2Br and Br photofragments that then interact with the solvent cage to give some recombination to produce either the parent dibromomethane or isodibromomethane photoproduct or some CH_2Br and Br fragments escape the solvent cage. This preliminary hypothesis is consistent with the available experimental data for A-band dibromomethane photochemistry (although there is admittedly little available at this time). This preliminary hypothesis can be further tested and the details on how the iso-CH_2Br-Br and CH_2Br photoproducts are formed from A-band photoexcitation of dibromomethane can be directly probed using ultrafast spectroscopy experiments such as femtosecond transient absorption experiments which have been very useful in investigating the closely related diiodomethane molecular system.[50−52] Ultrafast vibrational spectroscopy experiments would also be very useful to better understand the structural changes and properties of the initially formed photoproduct species and how they evolve into the CH_2Br and iso-CH_2Br-Br photoproducts we have observed on the nanosecond time scale. Further investigations (both theoretical and experimental) should prove rewarding for dihalomethane molecular systems such as dibromomethane, diiodomethane and others in order to better understand solvent−solute interactions and caging effects on their photodissociation/photoisomerization reactions in condensed phases.

Acknowledgment. This work was supported by grants from the Committee on Research and Conference Grants (CRCG), the Research Grants Council (RGC-HKU 509/96P and 7098/98P) of Hong Kong, the Hung Hing Ying Physical Sciences

Research Fund and the Large Items of Equipment Allocation 1993-94 from the University of Hong Kong.

References and Notes

(1) Simmons, H. E.; Smith, R. D. *J. Am. Chem. Soc.* **1959**, *81*, 4256.
(2) Blomstrom, D. C.; Herbig, K.; Simmons, H. E. *J. Org. Chem.* **1965**, *30*, 959.
(3) Pienta, N. J.; Kropp, P. J. *J. Am. Chem. Soc.* **1978**, *100*, 655.
(4) Kropp, P. J.; Pienta, N. J.; Sawyer, J. A.; Polniaszek, R. P. *Tetrahedron* **1981**, *37*, 3229.
(5) Kropp, P. J. *Acc. Chem. Res.* **1984**, *17*, 131.
(6) Friedrich, E. C.; Domek, J. M.; Pong, R. Y. *J. Org. Chem.* **1985**, *50*, 4640.
(7) Friedrich, E. C.; Lunetta, S. E.; Lewis, E. J. *J. Org. Chem.* **1989**, *54*, 2388.
(8) Durandetti, S.; Sibille, S.; Périchon, J. *J. Org. Chem.* **1991**, *56*, 3255.
(9) Class, Th.; Ballschmiter, K. *J. Atmos. Chem.* **1988**, *6*, 35.
(10) Klick, S.; Abrahamsson, K. *J. Geophys. Res.* **1992**, *97*, 12683.
(11) Heumann, K. G. *Anal. Chim. Acta* **1993**, *283*, 230.
(12) Moore, R. M.; Webb, M.; Tokarczyk, R.; Wever, R. *J. Geophys. Res.-Oceans* **1996**, *101*, No. C9, 20899.
(13) Carpenter, L. East Atlantic Spring Experiment (EASE), 1997 campaign. See also ref 14.
(14) Mössigner, J. C.; Shallcross, D. E.; Cox, R. A. *J. Chem. Soc., Faraday Trans.* **1998**, *94*, 1391.
(15) Molina, L. T.; Molina, M. J.; Rowland, F. S. *J. Phys. Chem.* **1982**, *86*, 2672.
(16) Gillotay, D.; Simon, P. C.; Dierickx, L. *Aeron. Acta* **1988**, *35*, 1.
(17) Mulliken, R. S. *J. Chem. Phys.* **1940**, *8*, 382.
(18) Ito, M.; Huang, P.-K. C.; Kosower, E. M. *Trans. Faraday Soc.* **1961**, *57*, 1662.
(19) Kawasaki, M.; Lee, S. J.; Bersohn, R. *J. Chem. Phys.* **1975**, *63*, 809.
(20) Schmitt, G.; Comes, F. J. *J. Photochem.* **1980**, *14*, 107.
(21) Kroger, P. M.; Demou, P. C.; Riley, S. J. *J. Chem. Phys.* **1976**, *65*, 1823.
(22) Riley, S. J.; Wilson, K. R. *Faraday Discuss. Chem. Soc.* **1972**, *53*, 132.
(23) Sparks, R. K.; Shobatake, K.; Carlson, L. R.; Lee, Y. T. *J. Chem. Phys.* **1981**, *75*, 3838.
(24) Van Veen, G. N. A.; Baller, T.; Devries, A. E.; Van Veen, N. J. A. *Chem. Phys.* **1984**, *87*, 405.
(25) Godwin, F. G.; Paterson, C.; Gorry, P. A. *Mol. Phys.* **1987**, *61*, 827.
(26) Black, J. F.; Powis, I. *Chem. Phys.* **1988**, *125*, 375.
(27) Zhu, Q.; Cao, J. R.; Wen, Y.; Zhang, J.; Huang, Y.; Fang, W.; Wu, X. *Chem. Phys. Lett.* **1988**, *144*, 486.
(28) Donohue, T.; Wiesenfeld, J. *J. Chem. Phys.* **1975**, *63*, 3130.
(29) Brewer, P.; Das, P.; Ondery, G.; Bersohn, R. *J. Chem. Phys.* **1983**, *79*, 720.
(30) Hess, W. P.; Kohler, S. J.; Haugen, H. K.; Leone, S. R. *J. Chem. Phys.* **1986**, *84*, 2143.
(31) Knee, J. L.; Khundar, L. R.; Zewail, A. H. *J. Chem. Phys.* **1985**, *83*, 1996.
(32) Khundar, L. R.; Zewail, A. H. *Chem. Phys. Lett.* **1987**, *142*, 426.
(33) Ogorzalek-Loo, R.; Haerri, H.-P.; Hall, G. E.; Houston, P. L. *J. Chem. Phys.* **1989**, *90*, 4222.
(34) Chandler, D. W.; Janssen, M. H. M.; Stolte, S.; Strickland, R. N.; Thoman, J. W., Jr.; Parker, D. H. *J. Phys. Chem.* **1990**, *94*, 4839.
(35) Triggs, N. E.; Zahedi, M.; Nibler, J. W.; Debarber, P. A.; Valentini, J. J. *J. Chem. Phys.* **1992**, *96*, 1822.
(36) Mastenbroek, J. W. G.; Taatjes, C. A.; Nuata, K.; Janssen, M. H. M.; Stolte, S. *J. Phys. Chem.* **1995**, *99*, 4360.
(37) Kang, W. K.; Jung, K. W.; Kim, D.-C.; Jung, K.-H. *J. Chem. Phys.* **1995**, *104*, 5815.
(38) Uma, S.; Das, P. K. *J. Chem. Phys.* **1996**, *104*, 4470.
(39) Koffend, J. B.; Leone, S. R. *Chem. Phys. Lett.* **1981**, *81*, 136.
(40) Cain, S. R.; Hoffman, R.; Grant, R. *J. Phys. Chem.* **1981**, *85*, 4046.
(41) Marvet, U.; Dantus, M. *Chem. Phys. Lett.* **1996**, *256*, 57.
(42) Zhang, Q.; Marvet, U.; Dantus, M. *J. Chem. Phys.* **1998**, *109*, 4428.
(43) Jung, K.-W.; Ahmadi, T. S.; El-Sayed, M. A. *Bull. Korean Chem. Soc.* **1997**, *18*, 1274.
(44) Baughcum, S. L.; Hafmann, H.; Leone, S. R.; Nesbitt, D. *J. Faraday Discuss. Chem. Soc.* **1979**, *67*, 306.
(45) Baughcum, S. L.; Leone, S. R. *J. Chem. Phys.* **1980**, *72*, 6531.
(46) Zhang, J.; Imre, D. G. *J. Chem. Phys.* **1988**, *89*, 309.
(47) Duschek, F.; Schmitt, M.; Vogt, P.; Materny, A.; Kiefer, W. *J. Raman Spectrosc.* **1997**, *28*, 445.
(48) Kwok, W. M.; Phillips, D. L. *J. Chem. Phys.* **1996**, *104*, 2529.
(49) Kwok, W. M.; Phillips, D. L. *Chem. Phys. Lett.* **1995**, *235*, 260.
(50) Schwartz, B. J.; King, J. C.; Zhang, J. Z.; Harris, C. B. *Chem. Phys. Lett.* **1993**, *203*, 503.
(51) Saitow, K.; Naitoh, Y.; Tominaga, K.; Yoshihara, K. *Chem. Phys. Lett.* **1996**, *262*, 621.
(52) Tarnovsky, A. N.; Alvarez, J.-L.; Yartsev, A. P.; Sundström, V.; Åkesson, E. *Chem. Phys. Lett.* **1999**, *312*, 121.
(53) Simons, J. P.; Tatham, P. E. R. *J. Chem. Soc. A* **1966**, 854.
(54) Mohan, H.; Rao, K. N.; Iyer, R. M. *Radiat. Phys. Chem.* **1984**, *23*, 505.
(55) Maier, G.; Reisenauer, H. P. *Angew. Chem., Int. Ed. Engl.* **1986**, *25*, 819.
(56) Maier, G.; Reisennauer, H. P.; Hu, J.; Schaad, L. J.; Hess, B. A., Jr. *J. Am. Chem. Soc.* **1990**, *112*, 5117.
(57) Andrews, L.; Prochaska, F. T.; Ault, B. S. *J. Am. Chem. Soc.* **1979**, *101*, 9.
(58) Mohan, H.; Iyer, R. M. *Radiat. Eff.* **1978**, *39*, 97.
(59) Mohan, H.; Moorthy, P. N. *J. Chem. Soc., Perkin Trans. 2* **1990**, 277.
(60) Sehested, J.; Ellermann, T.; Nielsen, O. J. *Int. J. Chem. Kinet.* **1994**, *26*, 259.
(61) Man, S. Q.; Kwok, W. M.; Phillips, D. L. *J. Phys. Chem.* **1995**, *99*, 15705.
(62) Kwok, W. M.; Phillips, D. L. *J. Chem. Phys.* **1996**, *104*, 9816.
(63) Man, S. Q.; Kwok, W. M.; Johnson, A. E.; Phillips, D. L. *J. Chem. Phys.* **1996**, *105*, 5842.
(64) Zheng, X.; Phillips, D. L. *J. Chem. Phys.* **1999**, *110*, 1638.
(65) Zheng, X.; Phillips, D. L. *J. Chem. Phys.* **1999**, *111*, 11034.
(66) Phillips, D. L. *Prog. React. Kinet. Mech.* **1999**, *24*, 223.
(67) Shoute, L. C. T.; Pan, D.; Phillips, D. L. *Chem. Phys. Lett.* **1998**, *290*, 24.
(68) Pan, D.; Shoute, D. L.; Phillips, D. L. *Chem. Phys. Lett.* **1999**, *303*, 629.
(69) Pan, D.; Phillips, D. L. *J. Phys. Chem. A* **1999**, *103*, 4737.
(70) Pan, D.; Shoute, L. C. T.; Phillips, D. L. *J. Phys. Chem. A* **1999**, *103*, 6851.
(71) Pan, D.; Shoute, L. C. T.; Phillips, D. L. *Chem. Phys. Lett.* **2000**, *316*, 395.
(72) Myers, A. B.; Li, B.; Ci, X. *J. Chem. Phys.* **1988**, *89*, 1876.
(73) (a) Frisch, M. J.; Trucks, G. W.; Schlegel, H. B.; Scuseria, G. E.; Robb, M. A.; Cheeseman, J. R.; Zakrzewski, V. G.; Montgomery, J. A.; Stratmann, R. E.; Burant, J. C.; Dapprich, S.; Millam, J. M.; Daniels, A. D.; Kudin, K. N.; Strain, M. C.; Farkas, O.; Tomasi, J.; Barone, V.; Cossi, M.; Cammi, R.; Mennucci, B.; Pomelli, C.; Adamo, C.; Clifford, S.; Ochterski, J.; Perterson, G. A.; Ayala, P. Y.; Cui, Q.; Morokuma, K.; Mailick, D. K.; Rabuck, A. D.; Raghavachari, K.; Foresman, J. B.; Cioslowski, J.; Orvitz, J. V.; Stefanov, B. B.; Liu, G.; Liashenko, A.; Piskorz, P.; Komaromi, I.; Gomperts, R.; Martin, R. L.; Fox, D. J.; Kieth, T.; Allaham, M.-A.; Peng, C. Y.; Nanayakkara, A.; Gonzalez, C.; Challacombe, M.; Gill, P. M. W.; Johnson, B. G.; Chen, W.; Wong, M. W.; Andres, J. L.; Head-Gordon, M.; Perlogle, E. S.; Pople, J. A. *Gaussian 98*, Revision A.1; Gaussian, Inc.: Pittsburgh, PA, 1998. (b) Becke, A. D. *J. Chem. Phys.* **1993**, *98*, 1372.
(74) Dunning, T. H., Jr. *J. Chem. Phys.* **1989**, *90*, 1007.
(75) Wilson, A. K.; Woon, D. E.; Peterson, K. A.; Dunning, D. H., Jr. *J. Chem. Phys.*, submitted for publication. Basis sets were obtained from the Extensible Computational Chemistry Environment Basis Set Database, Version 1.0, as developed and distributed by the Molecular Science Computing Facility, Environmental and Molecular Sciences Laboratory which is part of the Pacific Northwest Laboratory, P.O. Box 999, Richland, WA 99352, and funded by the U.S. Dpartment of Energy. The Pacific Northwest Laboratory is a multiprogram laboratory operated by Battelle Memorial Institute for the, U.S. Department of Energy under contract DE-AC06-76RLO 1830. Contact David Feller or Karen Schuchardt for further information.
(76) Bauernschmitt, R.; Ahlrichs, R. *Chem. Phys. Lett.* **1996**, *256*, 454.
(77) Zheng, X.; Phillips, D. L. Manuscript in preparation.
(78) Yamada, C.; Hirota, E. *J. Mol. Spectrosc.* **1986**, *116*, 101.
(79) Villenave, E.; Lesclaux, R. *Chem. Phys. Lett.* **1995**, *236*, 376.
(80) Smith, D. W.; Andrews, L. *J. Chem. Phys.* **1971**, *55*, 5295.
(81) Andrews, L.; et al. *J. Am. Chem. Soc.* **1979**, *101*, 7158.
(82) Myers, A. B.; Mathies, R. A. In *Biological Applications of Raman Spectroscopy*; Spiro, T. G., Ed.; Wiley: New York, 1987; Vol. 2, pp 1−58.
(83) Myers, A. B. In *Laser Techniques in Chemistry*; Myers, A. B., Rizzo, T. R., Eds.; Wiley: New York, 1995; p 325.
(84) Zheng, X.; Phillips, D. L. *Chem. Phys. Lett.* **2000**, *316*, 524.
(85) Zheng, X.; Phillips, D. L. *J. Phys. Chem. A* **2000**, *104*, 6880.
(86) Schmitt, G.; Comes, F. J. *J. Photochem. Photobiol. A* **1987**, *41*, 13.
(87) Lee, S. J.; Bersohn, R. *J. Phys. Chem.* **1982**, *86*, 728.
(88) Butler, L. J.; Hintsa, E. J.; Lee, Y. T. *J. Chem. Phys.* **1986**, *84*, 4104.
(89) Butler, L. J.; Hintsa, E. J.; Shane, S. F.; Lee, Y. T. *J. Chem. Phys.* **1987**, *86*, 2051.